Indian Journal of Pure & Applied Physics
Vol. 61, January 2023, pp. 43-56
DOI: 10.56042/ijpap.v61i1.66048

A New Adaptive OMP-MAP Algorithm-based Iterative Sparse Channel Estimation for OFDM Underwater Communication

Anand Kumar* & Prashant Kumar

Department of Electronics and Communication Engineering, National Institute of Technology Jamshedpur, Jharkhand, 831 014, India

Received 31 August 2022; accepted 21 December 2022

A sparse channel estimation approach based on doubly spread underwater acoustic (UWA) channels is widely used to detect coherent acoustic orthogonal frequency division multiplexing (OFDM) signals. A new time-domain channel estimation (CE) technique for OFDM based UWA communication with Rician fading is used to exploit the channel sparsity. First, to improve the estimation accuracy in high noise conditions, we have exploited the channel sparsity to generate a closed-form equation for the termination condition. Then, in low-level noise instances, the additional criterion to balance estimation accuracy and computing costs has been established. By incorporating these two requirements within the orthogonal-matching-pursuit (OMP) structure, an adaptive-OMP (AOMP) algorithm has been proposed. The AOMP and maximum a posteriori probability (MAP) techniques are combined to provide a computationally efficient, and a new AOMP-MAP scheme for estimating the sparse complex channel path gain has been proposed. Further, The minimum variance unbiased estimator is used to improve the proposed CE technique. Exploiting the experimental channel data, computer simulations reveal that the proposed CE technique obtains the outstanding outcomes.

Keywords: Underwater acoustic communication; Orthogonal frequency division multiplexing; Channel estimation; Sparsity; Adaptive orthogonal matching pursuit; MAP estimation

1 Introduction

Underwater communications (UWC) systems have recently gained considerable attention since they are critical for novel uses, including deep-sea mining, underwater environment monitoring, and underwater rescues, among others. For UWC, many media have been investigated (including acoustic, optical, and magnetic induction) in the literature reported previously. As compared to other media, acoustic waves have relatively high propagation properties, making them a viable choice for wide-area connection[1].

While acoustic waves are recommended for UWC systems, it has a lot of limitations, including reflections, large propagation loss, and low propagation speed. As a result of the low propagation speed of the acoustic signal, the Doppler Effect[2,3] may quickly reveal itself. Consequently, underwater acoustic (UWA) communications encounter a time-varying doubly selective channel that changes over time. The UWA channel is doubly distributed in both the delay and Doppler domains because of its multipath propagation and time-varying nature[4]. In the literature, this is referred to as being doubly selective in both the delay and Doppler domains. If delay-Doppler spread in time-varying UWA channels is to be combated effectively, it is necessary to accurately estimate the multipath delay as well as Doppler frequency and channel gain, which is a difficult challenge for high-speed UWA communications[4,5]. A feature of the UWA system is its wide frequency range, which is necessary for efficient acoustic propagation. Due to the wideband nature of the system, significant delay spreads typically impact UWA channels, resulting in inter symbol interference (ISI) covering a huge sum of symbol intervals. Additionally, the channel impulse response (CIR) is sparse in nature since few propagation paths carry significant energy. Thus, a realistic modem and subsequent channel model should take into account a sparse CIR, Doppler shifts, frequency-dependent path loss, and spreading (among other factors)[6].

A. Review of Existing Works

In recent years, UWA communications systems have been extensively investigated taking cyclic prefix orthogonal frequency division multiplexing

*Corresponding author: (E-mail: 2019rsec012@nitjsr.ac.in)

(CP-OFDM), a multicarrier transmission technique into account, to overcome the harsh underwater channel. For the CP-OFDM system, a number of benefits over traditional single-carrier systems exist. These include robustness against multipath channels, excellent spectral efficiency, and the possibility of implementing low-cost transceivers[7]. The fact that the CP-OFDM system is capable of converting a multipath channel in the time domain into a one-tap response for each subcarrier in the frequency domain confirms its robustness against a multipath channel on its operation. Therefore, precise channel estimation is required for the CP-OFDM system to provide proper equalization and data detection[8].

UWA-OFDM situations typically fail to function with conventional channel estimating methods like least square (LS), minimum mean square error (MMSE), and linear-MMSE (LMMSE) because of the inherent sparsity of the UWA channel. Since the UWA channel is sparse, it is well-known that channel estimation methods based on CS take this sparsity into account while estimating channel state information (CSI)[9]. With the orthogonal matching pursuit (OMP), the most typical of the others, significant estimation accuracy may be achieved at a minimal computational cost. In the case of a doubly selective channel, the authors have proposed an OMP-based technique for estimating channel coefficients without any prior CSI knowledge[10]. To estimate Doppler shifts in UWA communication systems using OFDM and a pilot, two methods are presented[11].

The notion of joint processing has been extensively explored in the context of UWA communications. In the beginning[12], for single-carrier UWA communication systems, an iterative receiver based on message-passing techniques is presented, in which equalization and decoding are rapidly performed several times. Although, channel estimation is performed using a maximum-likelihood (ML) technique and is dependent on training symbols. In severe inter-carrier interference (ICI) circumstances, an equalization technique has been developed in which an iterative receiver gradually raises the so-called ICI span parameter to enhance the channel estimation[13]. In situations with large Doppler spread, need extra pilots to estimate the channel[13,14]. An alternate scheme to ICI reduction, the use of several Partial fast Fourier transform (FFT) demodulation (PFD) instead of single full FFT demodulation (FFD) has been introduced[15,16]. Under the highly distorted underwater channel, the Partial FFT (PFFT) demodulation has been proposed to mitigate ICI. The substantial temporal changes in UWA channels, on the other hand, reduce the efficiency of OFDM in the receivers[17]. Further, the PFFT demodulation system has been suppressed in a weighted-type fractional Fourier transform (WFRFT) based hybrid carrier to mitigate the ICI[16]. Moreover, PFFT demodulation is proposed in MIMO-OFDM. The adaptive algorithm is used for single-window channel estimation[18]. Further, Iterative receivers for time-domain and frequency-domain equalization have been designed for single-carrier multiple-input multiple-output (MIMO) UWA communication systems. UWA channel information is required to compute MMSE coefficients for channel-estimation based turbo equalization, which may either be done by using a linear equalizer[19,20] or by using decision-feedback equalizer[21-23]. The frequency-domain turbo equalization (FDTE) significantly reduces the complexity while maintaining the same level of performance as time-domain turbo equalization (TDTE)[20] A more precise CSI estimate may be obtained using iterative channel estimation, which makes use of both soft-decision symbols and pilots in the first stages of the estimation process. A method for iterative sparse channel estimation and data detection using PFD is presented for OFDM UWA communication systems operating in double spread channels[24].

This paper investigates the estimation of sparse channel in cyclic prefix based OFDM (CP-OFDM) systems. Specifically, we focus on our previously used CP-OFDM design (Berger *et al*.[14], Yerramalli *et al*.[15], Mason *et al*.[25], Kumar and Kumar[26]. Yan *et al*.[7]), which employs a block-by-block receiver, in which each OFDM symbol is demodulated independently and coherently based on pilot subcarriers placed between the data subcarriers. The key points of the paper are briefly summarized next. As seen in Table 1, our contributions to the current state of the art are clearly compared.

The main contributions of this paper are as follows;

1. Sparse channel estimation has been applied to the partial interval demodulators (PID) outputs to solve the challenge of estimating the doubly-spread channel in cyclic prefix based OFDM system. Multipath channels are supposed to have Rician fading whereas Rayleigh fading are assumed by Panayirci *et al*.[27].
2. To improve the estimation accuracy in high noise conditions, the sparsity to generate a closed-form equation for the termination condition, has been

Table 1 — Our contributions in contrast to the state-of-the-art

Techniques	Berger *et al.*[14]	Huang *et al.*[13]	Yerramalli *et al.*[15]	Arunkumar *et al.*[24]	Panayirci *et al.*[27]	Yin *et al.*[28]	Chen *et al.*[1]	Proposed
Rician fading	×	×	×	×	√	×	×	√
Doubly spread channel estimation	×	×	×	√	√	×	×	√
Minimum variance unbiased estimator	×	×	×	×	×	×	×	√
Adaptive OMP-MAP algorithm	×	×	×	×	×	×	×	√
Partial FFT demodulation	×	×	√	√	×	√	×	√
MMSE equalizer	√	×	×	√	√	×	√	√

exploited. Then, in low-level noise instances, the additional criterion to balance estimation accuracy and computing costs has been established. By incorporating these two requirements within the OMP structure, an adaptive-OMP (AOMP) algorithm has been proposed.

3. By combining the AOMP and MAP algorithms, a new channel estimation scheme referred to as AOMP-MAP for sparse complex channel path gains have been proposed.
4. Iteratively recovering the channel and detecting the data symbols are two stages of our proposed system. To recover information from sparse channels, a new low complexity technique based on the idea of minimum variance unbiased estimator has been presented.
5. The proposed scheme has a significantly lower BER than previous methods in highly Doppler-spread scenarios, as demonstrated by extensive numerical simulations.

This paper is organized as follow: in Section 2, we develop the OFDM-based UWA communication systems are presented, along with the underwater primary channel characteristics and the noise level that it encounters in real life. In section 3, partial interval demodulation is explained to solve the challenge of input-output data model based on OFDM system. In the section 4, a new channel estimation technique is proposed based on AOMP-MAP structure which is the combination of AOMP and MAP technique for estimating the channel path gain. Further minimum variance unbiased estimator (MVUE) has been defined for improve the channel estimation process. In the section 5, we have provided the performance results based on proposed schemes and environmental parameters and conclude in section 6.

Notation: $[a]^+ \triangleq max(0, a)$. $\otimes$ represents the linear convolution.

2 System Model

In the UWA communication scenario, we consider a pilot-assisted OFDM-based system with K subcarriers. The source node S transmits data to the destination node D. We initially analyze a canonical channel model to investigate the impact of channel dispersion on the performance of the OFDM systems. It has no specific physical rationale but imitates an unsatisfactory case from a communication system[28] and helps us to develop general trends regarding the durability of the OFDM system against channel dispersion. Multipath propagation, generally with additional significant paths, characterizes the UWA channel between source and destination nodes, resulting in a sparse multipath channel model. The parametric model of the channel decreases the dimensions of the channel estimation problem and can produce higher performances than the non-parametric channel model-based estimators. The time-varying UWA CIR is sparse and characterized by

$$h(t,\tau) = \sum_{p=1}^{P} A_p(t)\delta\left(\tau - \tau_p(t)\right); \quad \ldots (1)$$

where, $\tau_p(t)$, $h_p(t)$ and P denoted the time-varying path delays, real-valued channel path, and number of non-zero paths, respectively. The path gains on each link will continue to vary from symbol to symbol over OFDM symbol transfer. It varies from symbol to symbol over OFDM symbol transfer, and the path gains on each link remain constant have been assumed. That is, $A_p(t) \approx A_p,\ p = 1, \cdots, P$. The time variations of the path delays are well approximated at the Doppler rate as $\tau_p(t) = \tau_p - \gamma_p t$ over the period of an OFDM symbol which is approximately linear[14,29]. The model in (1) only covers reliable channel path amplitudes of h_p acquired via a method of ray tracing.

Nevertheless, the diffuse multipath elements, $A_p^{(i)}, i = 1, 2, \cdots,$ are diffracted or scattered by the

rough sea and the bottom surface with the random phase $\tau_p^{(i)}, i = 1, 2, \cdots$. Therefore, a statistical description of the random channel tap variation in time needs to be increased. The analysis is limited to short-term statistical characterizations due to their non-stationarity. The CIR equivalent is therefore sparse, with every channel path performing as a randomly-varying low-pass filter with added Doppler spreading and shifting, which is characterized by

$$h_b(t,\tau) = \sum_{p=1}^{P} h_p e^{j2\pi f_c \gamma_p t} \delta\left(\tau - \tau_p(t)\right); \quad \ldots(2)$$

where, f_c is the carrier frequency and the sparse CIR given by $h_p = \sum_i h_p^{(i)} e^{-j2\pi f_c \tau_p^{(i)}}$. In this paper, the channel path gain is defined by rician distribution where h_p are complex Gaussian random variable (RV) with μ_p mean and σ_p^2 variance. γ_p denotes the Doppler effect which is divided into a non-zero valued Doppler shift and Doppler spread. In addition, the p^{th}tap rician-k factor is the power ratio of the power in mean component to the diffused component, i.e. $k_p = \mu_p^2 / \sigma_p^2$, each rician channel tap can be determined as follows

$$h_p = \sqrt{\frac{k_p \omega_p}{k_p + 1}}\left(\frac{1+j}{\sqrt{2}}\right) + \sqrt{\frac{\omega_p}{k_p + 1}}\check{h}_p, \quad \ldots(3)$$
$$p = 1,2,\cdots,P;$$

where $\omega_p = E\left\{\left|h_p\right|^2\right\} = 2\left(\mu_p^2 + \sigma_p^2\right)$ and $\sum_{p=1}^{P} \omega_p = 1$. $\check{h}_p \sim CN(0,1)$is complex Gaussian RV.

We consider a pilot-assisted OFDM-based UWA communication scenario. Let T be the duration of the symbol and T_g be the guard interval. Therefore k^{th}subcarrier will be at the frequency

$$f_k = f_c + \frac{k}{T}, \qquad k = -\frac{K}{2}, \cdots, \frac{K}{2} - 1. \quad \ldots(4)$$

The CP is an excellent approach to ensure the orthogonality of the carrier in a delayed-dispersive (frequency-selective) environment. Delay dispersion can be another source of ICI if CP is shorter than the maximum excess delay of the channel. The null subcarriers S_N are not significant in terms of performance but are useful to calculate ICI as the double-spread channel in the frequency domain remains no longer diagonal. Let k^{th} carrier be the transmit symbols. The transmitted signal is then:

$$\tilde{x}(t) = \sqrt{\frac{1}{T}} Re\left\{\left[\sum_{k \in S_P \cup S_D} s[k] e^{j2\pi \frac{k}{T} t}\right] e^{j2\pi f_c t}\right\};$$
$$t \in \left[-T_g, T\right] \quad \ldots(5)$$

where, $Re\{\cdot\}$ denotes the real value. S_D and S_P denote the data subcarrier and pilot subcarrier respectively. The disjoint set of S_D, S_P and S_N partition the K available subcarrier. Determined on the base of the number of subcarriers, the roll-off factor of the overall root raised cosine filter is computed within the flat region of both sender and receiver response. The total overall OFDM symbol duration is $T_{SYM} = T + T_{CP}$. Therefore the received passband signal is reported as

$$\tilde{z}(t) = \sqrt{2} Re\{(\tilde{x}(t) \otimes h_b(t,\tau)) e^{j2\pi f_c t}\} + \tilde{n}(t);$$
$$= \sqrt{2} Re\left\{\left(\sum_{p=1}^{P} h_p\, e^{j2\pi f_c \gamma_p t}\, \tilde{x}\left(\left(1+\gamma_p\right)t - \tau_p\right)\right) e^{j2\pi f_c t}\right\} + \tilde{n}(t); \quad \ldots(6)$$

where, $\tilde{n}(t) = \sqrt{2} Re\left\{n(t) e^{j2\pi f_c t}\right\}$, γ_p is represented the Doppler effect which is allocated into mean Doppler shift with a non-zero value.

The recipient samples the passband signal directly with a relatively low carrier frequency in conventional UWA communication systems. As a result, downshifting and Doppler shift estimates, channel estimation, and compensation are commonly performed in the digital domain for resampling passband-to-baseband signals. With resampling factor $1 + \hat{\gamma}$, the principal Doppler scaling effect is removed, and this leads to the resampled signal $\tilde{z}_{RS}(t) = \tilde{z}\left(t/(1+\hat{\gamma})\right)$. The signal is resampled at the receiver with a factor $\hat{\gamma}$ which is equivalent to a coarse Doppler estimation. Therefore the received baseband signal is reported[15, 30, 31],

$$\tilde{z}_{RS}(t) = Re\left\{e^{j2\pi f_c t} \sum_{p=0}^{P-1} h_p e^{j2\pi f_c \beta_p t}\, \tilde{x}\left(\left(1+\beta_p\right)t - \tau_p\right)\right\} + \tilde{n}_{RS}(t); \quad \ldots(7)$$

where,

$\beta_p = \frac{\gamma_p - \hat{\gamma}}{1+\hat{\gamma}}$ and $\tilde{n}_{RS}(t) = \tilde{n}\left(\frac{t}{(1+\hat{\gamma})}\right)$.

The Doppler shift is due to the relative movement of the transmitter and the receiver system, where different travel paths and receiver angle shifts are induced by Doppler spread. The new residual Doppler shift β_p on each path is introduced in (7). The resampling in (7) removes the non-zero mean of γ_p. After compensation $\hat{\gamma}$, the β_p are found to be spread around zero between$[-b_{max}, b_{max}]$.

Before channel estimation, the mean Doppler shift should be eliminated from the signaling data. The testing of raw acoustic data is done using a resampling factor, which indicates a nominal sound velocity for c = 1500m/s. When using positive velocities, it is typical to use signs that represent a wide range of times, which is known as a signal expansion. The Doppler shift is omitted from the channel estimation $\hat{h}(t,\tau)$.

The reason behind the elimination of mean Doppler shift β_p is that it reduces channel rigorous measuring mistakes. However, when Watermark recovers the simulated packets, mean shift restores instant Doppler spreading, and time-variable Doppler shifts β_p around the mean value are replicated in a direct replay[32]. These packets are resampled by a resampling factor $1+\hat{\gamma}$. This ensures that the input signal $x(t)$ in the simulated channel is used to transfer all effects of Doppler from the channel sensor signal in the real channels.

3 DEMODULATION

B. Conventional OFDM Demodulation

In a conventional receiver, the cyclic prefix is eliminated, and the received signal is translated into the frequency domain following time and frequency synchronization

$$y_k = \sqrt{\frac{1}{T}}\int_0^T \tilde{z}_{RS}(t)e^{-j2\pi f_k t}\,dt$$
$$= \frac{1}{T}\sum_{l\in S_D\cup S_P} s[l]\int_0^T \underbrace{\left[\sum_{p=1}^{P} h_p e^{-j2\pi f_l \tau_p(t)}\right]}_{H_l(t)} e^{j2\pi(\Delta f+\beta_p f_l)t} + n_k. \quad \ldots (8)$$

Here, $H_l(t)$ represents the time-varying frequency response of the k^{th} subcarrier, n_k is the AWGN with zero mean and variance N_0. $\Delta f = f_l - f_k$. In (8), the time-varying channel causes ICI. Assuming $H_l(t)$ is time-invariant, each subcarrier's reception signal simplifies to $y_k = d_k H_k + n_k$ to allow one-tap equality and optimal identification of a symbol by symbol. Compared to the original channel, the Doppler spread can be slightly decreased in a replay channel[33].

C. Partial FFT Demodulation (PFD)

In PFD, the convenient period of the OFDM symbol $[0,T]$ is divided into M non-overlap intervals, with each windowed segment of signals is subjected to a Fourier transform. The Fourier transform output for the k^{th} and m^{th}subcarriers and the windowed block respectively, denoted as the PID output, can be written as,

$$y_k^{(m)} = \sqrt{\frac{1}{T}}\int_{\frac{(m-1)T}{M}}^{\frac{mT}{M}} \tilde{z}_{RS}(t)e^{-j2\pi f_k t}\,dt$$
$$= \frac{1}{T}\sum_{l\in S_D\cup S_P} s[l] \int_{\frac{(m-1)T}{M}}^{\frac{mT}{M}} \left[\sum_{p=0}^{P-1} h_p^{(m)} e^{-j2\pi f_l \tau_p^{(m)}}\right] e^{j2\pi(\Delta f+\beta_p f_l)t}\,dt + n_k^{(m)}; \quad \ldots (9)$$

where, $m = 1,2,\cdots M$ and $s \in C^K$. We use this assumption by using the midpoint value of the function to approximate the time-varying frequency response in each interval T/M. The received signal (9) can now be simplified as

$$y_k^{(m)} \approx \sum_{l\in S_D\cup S_P} s[l]\, H_l^{(m)} I_{l-k}^{(m)} + n_k^{(m)}; \quad \ldots(10)$$

where,

$$H_l^{(m)} = \sum_{p=1}^{P} h_p^{(m)} e^{-j2\pi f_l \tau_p^{(m)}}; \quad \ldots (11)$$

where again $H_l^{(m)}$ denotes midpoint of frequency response, $h_p^{(m)}$, the channel impulse response, and $\tau_p^{(m)}$, the path delay on the interval $\left[(m-1)\frac{T}{M}, \frac{mT}{M}\right]$. The function $I_i^{(m)}$ captures the effect of partial integration over the m^{th} interval can be evaluated as

$$I_i^{(m)} = \frac{1}{T}\int_{\frac{(m-1)T}{M}}^{\frac{mT}{M}} e^{j2\pi(\Delta f+\beta_p f_l)t}\,dt\,;$$
$$I_i^{(m)} = \frac{1}{M} e^{\frac{j2\pi i(2m-1)}{2M}} \text{sinc}\left((l-k)\frac{1}{T}+\beta_p f_l\right),$$
$$i = -(K-1),\cdots,(K-1) \quad \ldots (12)$$

where, $\text{sinc(a)} = \frac{\sin(\text{a})}{\text{a}}$. The eq.(12) has initial properties that $I_0^{(m)} = \frac{1}{M}$, where $m = 1,2,\cdots,M$, and the sum of m value of $\sum_{m=1}^{M} I_i^{(m)} = 0\ \forall i \neq 0$. For the k_{th} subcarrier $I_k = \left[I_k^{(1)},\ I_k^{(2)},\ \cdots,\ I_k^{(M)}\right]^T$ is containing the partial interval integration coefficients. It is noted that $I_0 = \frac{1}{M}[1,1,\cdots,1]^T$ and $I_k^H I_0 = 0\ \forall k \neq 0$, which succinctly conveys that the OFDM subcarrier is orthogonal to each other.

D. Input-Output Data Model

The input-output relationship can be written by stacking the received vector $Z_{RS}^{(m)} \in C^K$, data symbols in $s \in C^K$ and noise vector $N_{RS}^{(m)} \in C^K$ across all the subcarriers:

$$Z_{RS}^{(m)} = H^{(m)}s + N_{RS}^{(m)},\quad m = 1,\cdots,M\,; \quad \ldots(13)$$

where,

$$Z_{RS}^{(m)} = \left[Z_{RS}^{m}[-K/2\,], Z_{RS}^{m}[-K/2\ +1],\cdots Z_{RS}^{m}[K/2\ -1]\right]^T \in C^K$$
$$s = \left[s_{-K/2}, s_{-K/2+1},\cdots s_{K/2-1}\right] \in C^K$$
$$N_{RS}^{(m)} = \left[N_{RS}^{(m)}[-K/2\,], N_{RS}^{(m)}[-K/2\ +1],\cdots N_{RS}^{(m)}[K/2\ -1]\right]^T \in C^K$$

and the $[k,l]^{th}$ element of $H^{(m)} = \sum_{p=1}^{P} h_p \Lambda_p^{(m)} \Gamma_p \in C^{K\times K}$ is determined in (11). Here $\Lambda_p^{(m)}$ is $K \times K$ matrix with $[k,l]^{th}$ entry $\left[\Lambda_p\right]_{k,l}^{(m)} = I_i^{(p)}[m]$, and Γ_p is $K \times K$ diagonal matrix which is represented as $\Gamma_p = e^{-j2\pi f_k \tau_p}$.

The output of conventional full interval demodulation is obtained by summing up all $Z_{RS}^{(m)}$, where $m = 1,2,\cdots,M$, then $Z_{RS} = \sum_{m=1}^{M} Z_{RS}^{(m)} = Hs + N$, where H and N are also obtained by summing up all $H^{(m)}$ and $N^{(m)}$, which are $H = \sum_{m=1}^{M} H^{(m)}$ and $N = \sum_{m=1}^{M} N^{(m)}$ respectively. Whenever the additive noise (7) is zero-mean circularly symmetric white Gaussian distributed, then the noise has also zero mean at full interval demodulation, a Gaussian with a $N_0 I$ covariance, where the variance of N_0 is defined as each component of n, and I is the $K \times K$ identity matrix. In (13), the noise is also zero-mean Gaussian distributed but not white, with covariance is given by

$$E\left[\eta_k^{(m)}\eta_k^{(m)*}\right] = \begin{cases} \frac{N_0}{M} e^{-\frac{j2\pi(k-l)(2m-1)}{2M}} sinc\left(\frac{k-l}{M}\right) & \text{for} m_1 = m_2 \\ 0 & \text{for} m_1 \neq m_2 \end{cases} \quad \ldots (14)$$

This means that the noise components are Gaussian and uncorrelated, so it is not correlated across partial FFT outputs for a given subcarrier. However, it is correlated across subcarriers for a fixed number of subcarriers. It is also clear that the channel matrix H as seen by the FID is diagonal when β_p is set to zero. Due to the severe Doppler spread, β_p are set to non-zero and high, therefore the channel matrix is not diagonal anymore, so that symbols at the output are mixed according to each subcarrier. Moreover, $\beta_p t$ can be approximated in a partial interval by $\beta_p t_m$, where $t_m \triangleq (2m-1)\frac{T}{2M}$ is the partial interval mid-point[7,15]. Now, the channel matrix can be written as

$$H^{(m)} = \frac{1}{M}\sum_{p=1}^{P} h_p e^{-\frac{j2\pi(k-l)(2m-1)}{2M}} sinc\left(\frac{k-l}{M}\right) e^{-j2\pi f_k(\tau_p-\beta_p t_m)}; \quad \ldots (15)$$

where $e^{-j2\pi f_k(\tau_p-\beta_p t_m)}$ is diagonal matrix with $(k,k)^{th}$ entry. From now on, we analyze PID data models with (13) outputs in which the channel matrix is specified (15), and the noise vector with a covariance matrix is zero mean which has been defined in (14).

4 Sparse Channel Estimation, Data Detection

Herein, we focus mainly on estimating a fast time-varying UWA channel based on the observation model in (13). The channel matrix $H^{(m)}$ is defined by N_P triplets $\left(h_p, \beta_p, \tau_p\right)$. We characterize the challenge of estimating the triplets of N_p, taking the PID output sequence $Z^{(m)} \in C^K, m = 1,2,\cdots,M$, as a sparse channel recovery problem.

$$Z^{(m)} = A^{(m)}x + N^{(m)}; \quad \ldots (16)$$

where,

$$x = \left[\left(x_A^{(1)}\right)^T, \cdots, \left(x_A^{(N_b)}\right)^T\right]^T, \quad \ldots (17)$$

and

$$A^{(m)} = \left[\Psi_1^{(m)}s, \Psi_2^{(m)}s, \cdots, \Psi_N^{(m)}s\right]; \quad \ldots (18)$$

where again, N_b is taken Doppler rate for β_p, which is $N_b = 2b_{max}/(\nabla\beta) + 1$. For the difference in value of b_{max}, the value of $\left(\nabla\beta \approx \sqrt{12} \times 10^{-5}\right)$ to neglect the equalization noise when compared with β_p's mean-square estimation error. The x is the vector of stacking coefficient for all candidate delays (N_τ) and Doppler scale β_i as $x_A^{(i)} = \left[A_1^{(i)}, \cdots, A_{N_\tau}^{(i)}\right]^T$.

Despite the sparsity of the channel vector x which is complex in nature, the generation of the dictionary matrix $A^{(m)}$ requisite information of the transmitted symbol vector s, is unknown at the receiver. The known pilot symbol vector $\hat{s} \in C^K$ at the pilot subcarrier location followed by null subcarrier. Further, unknown data symbols are initialized at the data subcarrier location S_D. $Z_{Sp}^{(m)}$is defining a sub-vector for (16) that reflect the position of the pilot subcarrier S_P, we have,

$$Z_{Sp}^{(m)} = \hat{A}_{Sp}^{(m)}x + e_{Sp}^{(m)}; \quad \ldots (19)$$

where,

$$\hat{A}_{Sp}^{(m)} = I_{Sp}\left[\Psi_1^{(m)}\hat{s}, \cdots \Psi_N^{(m)}\hat{s},\right] \in C^{|Sp|\times N}; \quad \ldots (20)$$

where again,

$$\left[\Psi_p\right]_{k,k}^{(m)} = \frac{1}{M}e^{-\frac{j2\pi\{(k-l)(2m-1)+f_k(\tau_p-\beta_p t_m)\}}{2M}} \operatorname{sinc}\left(\frac{k-l}{M}\right), \quad \ldots (21)$$

$I_{Sp} \in R^{|Sp|\times K}$ is the $K \times K$ identity submatrix matrix consisting of its rows indexed by S_P. The $e_{Sp}^{(m)} = \Delta A_{Sp}^{(m)}x + N_{Sp}^{(m)}$ is the effective noise which includes the $\Delta A_{Sp}^{(m)} = I_{Sp}\left[\Psi_1^{(m)}(s - \hat{s}), \cdots \Psi_N^{(m)}(s - \hat{s})\right]$ error in the dictionary estimates.

When the Doppler spreads are $b_{max} = 10 \times 10^{-4}$ and $b_{max} = 0.5 \times 10^{-4}$, Fig. 1 and 2 depict the singular value dictionary matrix $A_{Sp}^{(m)}$ equivalent to the PID outcome for pilot subcarriers, respectively. An additional plot of the dictionary matrix $A_{Sp}^{(m)}$

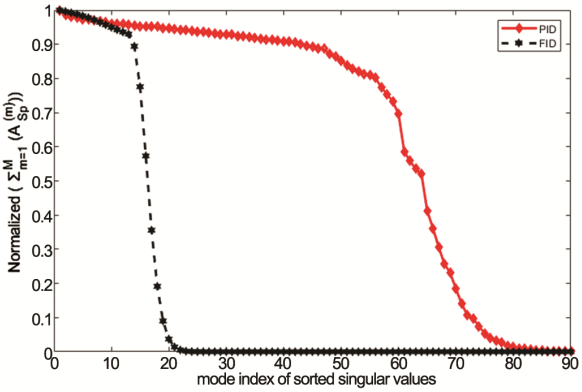

Fig. 1 — Dictionary matrices equivalent to PID and FID outputs with singular values decomposition where b_{max} is set to 10×10^{-4}.

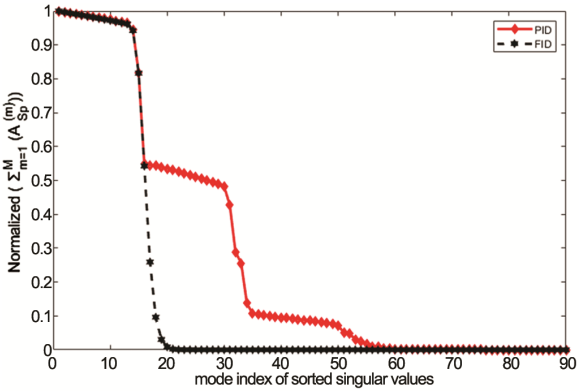

Fig. 2 — Dictionary matrices equivalent to PID and FID outputs with singular values decomposition, where b_{max} is set to 0.5×10^{-4}.

values for pilot subcarriers' FID observations are presented in this picture. Using only the PID's pilot measurements instead of the FID's can lead to improved channel estimations. The k-rank of the dictionary matrix rank $\left(A_{Sp}^{(m)}\right)$ must be less than or equal to $\min(M|S_P, K)$. So, the dictionaries are constructed for high Doppler spread, the numerical rank of the PID is clearly superior to the numerical rank of the FID. More accurate channel estimation may be achieved by employing the observation sequence from PIDs, which is equivalent to the output of oversampling of the OFDM receiver.

E. Adaptive OMP (AOMP) Algorithm

The OMP is designed to recover the sparse signal, which ignores the additive noise influence[14,29]. In most cases, however, it is impossible to ignore the noise due to the significant impact it would have on the accuracy of channel estimation techniques. Considering that, Eq. (16) can be rewrite

$$z = \Upsilon x + n = \Upsilon(x + \Upsilon^{-1}n) = \Upsilon(x + x_e); \quad \ldots (22)$$

where $z \equiv Z^{(m)}$, $\Upsilon \equiv [v_0, v_1, \cdots, v_{L-1}]$, v_l is the l^{th}column of $A^{(m)}$ in (18) and $n \equiv N^{(m)}$. The x_e is mean equivalent tap coefficients, which is resulted by the adaptive noise.

As a result, one possible suggested solution for modifying the OMP is to choose a threshold Φ for the estimated channel coefficient$x$. When x at the j^{th} iteration is lower than the threshold Φ, then the iteration will be stopped and assume that the remaining estimated taps are produced by noise. Further, by Wang *et al*. the detailed derivation of threshold Φ is presented [34]. So, the Moore-Penrose pseudo-inverse matrix Υ^{+} is replaced to Υ^{-1}. Thus the mean equivalent tap coefficients which is represented by the additive noise, can be written as

$$x_e = \Upsilon^{-1}n = \Upsilon^{+}n; \quad \ldots (23)$$

where $\Upsilon^{+} = \Upsilon^{H}(\Upsilon\Upsilon^{H})^{-1}$. Eq. (23) after simplification, can be rewritten as

$$x_e = \frac{1}{S_p}\Psi^{H}s^{-1}n. \quad \ldots (24)$$

Considering that s is the transmitted signal which is a diagonal matrix. Furthermore, the mean value of x_e is equal to zero because the Gaussian vector n and the measurement matrix Υ are independent to each other. In light of that, the standard deviation can be calculated as

$$\sigma = \sqrt{\left(\frac{1}{S_p}\Psi^{H}s^{-1}n\right)^{H}\left(\frac{1}{S_p}\Psi^{H}s^{-1}n\right)}$$
$$= \sqrt{\left(\frac{1}{S_p}\right)^{2} n^{H}(s^{-1})^{H}\Psi\Psi^{H}s^{-1}n}$$
$$\approx \sqrt{\frac{S_p\sigma_s^2\sigma_n^2}{S_P^2}} = \frac{\sigma_s\sigma_n}{\sqrt{S_P}} \quad \ldots (25)$$

In addition, considering the Gaussian distribution, the random value lie within the range of two standard deviation which is away from the mean value. So, the threshold is set to $\Phi = \sigma\sqrt{\frac{m}{l}}$, which means the iteration procedure will stop when the estimation of the channel reaches to the threshold value. We summarized our AOMP algorithm in Table 2.

F. Channel Path Gain Estimation

After acquiring information on the path delays and Doppler spread information from the OMP method, we can use the MAP approach to estimate the channel path gains in the most optimum manner possible. In order to make the notation in a simple manner, we rewrite (16) as follows:

Table 2 — AOMP algorithm

1.	Input
	Received symbol z
	Dictionary matrix Υ
	Fixed value σ
2.	Output
	Reconstructed signal $\hat{x}$
3.	Initialization
	Resuidal vector r= z
	Iteration number t=1,
	Index set$\Lambda = \phi$.
4.	While $\hat{x}_{t^*} \geq 2\sigma$ or $\|r_t\|^2 \geq 0.003\|z\|^2$ do
5.	Find index $t^* = \arg\max_{j=1,2,\cdots,N} \| < r_{t-1}, a_j > \|$.
6.	Update index set $\Lambda_t = \Lambda_{t-1} \cup t^*$.
7.	Compute $\hat{x}_{t^*} = \left(\Upsilon_{t^*}^{H}\Upsilon_{t^*}\right)^{-1}\Upsilon_{t^*}^{H}r_{t-1}$.
8.	Update residual vector $r_t = r_{t-1}\Upsilon_{t^*}\hat{x}_{t^*}$
9.	$t = t + 1$.
10.	end while

$$z = \Upsilon x + n; \quad \ldots (26)$$

where $z \equiv Z^{(m)}$, $\Upsilon \equiv [v_0, v_1, \cdots, v_{L-1}]$, $v_l$is the l^{th}column of $A^{(m)}$ in (18) and $n \equiv N^{(m)}$. Now the notation $\alpha_p = \sigma_p^2$ and $\eta \equiv \frac{1}{\sigma_N^2}$ are used in the following derivations. As stated before, we presumptively assume that the channel path gains follow a Rician distribution with x_p being complex Gaussian random variables with Rician factor $\kappa = \mu_p^2/\alpha_p$, where real and imaginary parts are independent of each other. As a result, the parametric form of the prior joint probability density function (pdf) of x can be written as

$$f(x|\tilde{\mu}, \tilde{\alpha}) = \prod_{p=1}^{P}\frac{1}{\pi\tilde{\alpha}_p}\exp\left(-\frac{1}{\tilde{\alpha}_p}|x_p - \tilde{\mu}_p|^2\right); \quad \ldots (27)$$

where, $\tilde{\mu}_p = \mu_p(1 + j)$ and $\tilde{\alpha}_p = 2\alpha_p$. The mean vector $\tilde{\mu} = \left[\tilde{\mu}_1, \tilde{\mu}_2, \cdots, \tilde{\mu}_p\right]^T$and variance vector $\tilde{\alpha} = \left[\tilde{\alpha}_1, \tilde{\alpha}_2, \cdots, \tilde{\alpha}_p\right]^T$are $2P$ parameters that specify the prior mean and variance of each channel coefficient x, respectively. According to the following (27), the posterior density of the channel coefficients vector is a complex Gaussian for given values of the parameters regulating the prior. Moreover, the MAP estimation for x can be written as

$$\hat{x}_{MAP} = arg\max_{x} f(x|z, \tilde{\mu}, \tilde{\alpha}) = \mu_x; \quad \ldots (28)$$

where $\mu_x = (\eta\Upsilon^*\Upsilon + \Lambda^{-1})^{-1}(\eta\Upsilon^* z + \Lambda^{-1}\tilde{\mu})$ and the posterior density of the channel coefficients vector $p(x|z,\tilde{\mu},\tilde{\alpha}) = \mathcal{CN}(\mu_x, \Gamma_x)$, where$\Gamma_x = (\eta\Upsilon^*\Upsilon + \Lambda^{-1})^{-1}$, is a complex Gaussian when the parameters regulating the prior are held constant. The Λ is a diagonal of $\tilde{\alpha}$ matrix. The $\Upsilon^*\Upsilon$are the banded matrix, and it is approximated as $\Upsilon^*\Upsilon = diag(\|v_1\|^2, \|v_2\|^2, \cdots \|v_P\|^2)$. Then matrix of Γ_x can be written as

$$\left(\Upsilon^*\Upsilon + \frac{1}{\eta}\Lambda^{-1}\right)^{-1} = diag(\lambda_1, \lambda_2, \cdots, \lambda_P); \quad \ldots (29)$$

with $\lambda_P = \left(\eta\|v_p\|^2 + 1/\tilde{\alpha}_p\right)^{-1}$.

G. Minimum Variance Unbiased Estimation (MVUE)

After recovering the sparse channel vector x, the channel matrix $H^{(m)}$ for each PFD output is generated (15). The MVUE algorithm is inspired by the linear minimum variance unbiased (LMVU) estimation and minimum variance spectrum estimation principal[35]. To understand the motivation for the MVUE, it is necessary to examine the MLE for the complex amplitude of a complex sinusoid in complex Gaussian noise. In order to get a nearly diagonal post-combined channel matrix, the estimations $H^{(m)}, m = 1,2,\cdots,M$ are weighted and merged. The mean vector $\tilde{\mu} = [\tilde{\mu}_1, \tilde{\mu}_2, \cdots, \tilde{\mu}_p]^T$ and variance vector $\tilde{\alpha} = [\tilde{\alpha}_1, \tilde{\alpha}_2, \cdots, \tilde{\alpha}_p]^T$ from (26), it follows that

$$p(z|x) \sim \exp\{-\eta\|z - \Upsilon x\|^2\}; \quad \ldots (30)$$

and $p(x|\mu,\alpha)$ is given by (27).

The ML estimate of $\mu$is now obtained by minimizing $\log p(z|\mu,\alpha)$. By kay, using $\log p(z|\mu,\alpha)$ derivative with respect to μ and setting the resultant gradient to zero and by applying the method mentioned[35], the following solution is obtained as

$$\hat{\mu}_{ML} = (\Upsilon_0^* R_{zz}^{-1}\Upsilon_0)^{-1}(\Upsilon_0^* R_{zz}^{-1} z); \quad \ldots (31)$$

where the inverse cross-correlation matrix R_{zz}^{-1} can be written as

$$R_{zz}^{-1} = \eta I_P - \eta\Upsilon\lambda\Upsilon^*; \quad \ldots (32)$$

where again, $\lambda = diag(\lambda_1, \lambda_2, \cdots, \lambda_P)$ with $\lambda_p = \left(\|v_p\|^2 + 1/(2\eta\alpha_p)\right)^{-1}$.

By substituting inverse cross-correlation matrix (R_{zz}^{-1}) into (31). The estimated expression for μ can be written as

$$\hat{\mu}_{ML} = \frac{1}{2}\begin{bmatrix} \|v_1\|^2 & 0 & \cdots & 0 \\ 0 & \|v_2\|^2 & \cdots & 0 \\ \vdots & \vdots & \ddots & \vdots \\ 0 & 0 & \cdots & \|v_P\|^2 \end{bmatrix} \Re\{\Upsilon_0^* z\}. \quad \ldots (33)$$

From (32) and (33), now in order to get the ML variance estimate ofα, and on maximizing the log-likelihood $\log p(z|\hat{\mu}_{ML},\alpha)$ with respect to α, we get

$$\begin{aligned} \arg\max_{\alpha} \log p(z|\hat{\mu}_{ML},\alpha) &= \sum_{p=1}^{P} \log\left(2\|v_p\|^2\alpha_p + \frac{1}{\eta}\right) \\ &- \eta\sum_{p=1}^{P}\left(|\theta_p|^2\lambda_p\right. \\ &\left. - \|z - \Upsilon_0\hat{\mu}_{ML}\|^2\right); \end{aligned} \quad \ldots (34)$$

where θ_p is the p^{th} component of the vector $\Theta \triangleq \Upsilon_0^*(z - \Upsilon_0\hat{\mu}_{ML})$. The ML estimate for α is obtained by taking the derivative of (34) to α_p, which equals zero, and solving the resultant equation as

$$\hat{\alpha}_{p,ML} = \left(\frac{\eta|\theta_p|^2 - \|v_p\|^2}{2\eta\|v_p\|^4}\right)^+; \quad \ldots (35)$$

Finally, using the decoupled expressions (33) and (35), we can estimate the prior pdf's mean and variance in an efficient manner. The MVUE algorithm is refining the channel estimation procedure by MAP-OMP. Using MAP-OMP based sparse channel estimation as a preliminary step, then the measurement covariance matrix and utilize it to generate an adaptive minimum variance weight vector have been estimated. It is important that each element in the channel vector be re-estimated using a weight vector since this will allow us to update the solution to only include indices for the lowest variance entries. Further, the subsequent equalization and data detection step is explained.

H. Equalization and data detection

In this section, we'll discuss the receiver equalization and data detection processes, using the received signal model from (13). The noise variance at the post-combiner output is $E[|\tilde{\eta}_k|^2] = N_0$. This is followed by recovering the equalized symbol values of soft data using an MMSE equalizer as

$$\hat{s} = dec\,[(HH^* + N_0 I)^{-1}H^*\tilde{z}]; \quad \ldots (36)$$

where, $dec(\cdot)$ is the operation of hard-thresholding to the signal constellation. By substituting the channel estimate $\left[\hat{h}_p, \left(\hat{\beta}_p, \hat{\tau}_p\right)\right]_{p=1}^{P}$ acquired during the OMP-MAP channel estimation step, the element of H is calculated from (15). After a post-combined demodulator has been used to recover the channel vector, it is possible to explore the data symbols by analyzing just the pilot subcarriers in the output of the PFD. When data symbols are detected, the ICI can be estimated more precisely, which in turn helps to reduce $\left\|\Delta A_{Sp}^{(m)} x\right\|_2$ in (19), which leads to more accurate channel estimations. However, because data subcarrier observations are not utilized for channel estimation, we employ measurements from both data and pilot subcarriers.

The dictionary matrix for the full interval as $A = \sum_{m=1}^{M} A^{(m)}$, with the estimated data symbol $\hat{s}$. Further, the channel vector is re-estimated from

$$z = \sum_{m=1}^{M} z^{(m)} = Ax + n. \quad \ldots (37)$$

We can deduct that the output of the full interval now includes all observations, including those from data subcarriers. Using (28) and (26), the post-combined channel matrix $\widehat{H}$ and the associated post-combined measurement $\tilde{\boldsymbol{z}}$ from the estimated channel vector have been constructed, and then the data is demodulated using the MMSE receiver in (36).

5 Numerical Simulations

In this section, the performance of the proposed channel estimation technique using the PFFT approach is evaluated. The CP-OFDM system model has been considered, and the parameters are listed in Table 3. The well-known experiment was conducted in 2008 by WHOI, named SPACE08. In previous simulation studies, the system's parameters matched those of the SPACE08 experiment which is shown in Fig. 3, and it has been frequently utilized for that purpose[21,36,37]. The underwater channel SPACE08 simulation parameter is shown in Table 4. In the presented simulation results, the Pilot symbols are spaced uniformly. Among the null subcarriers, A half is positioned at the signal band edges, and the rest are equispaced between the data[24,38,39].

The Simulation model has been presented for UWA communication. The sparse channels with a small number of distinct pathways with an inter-arrival time of 1ms are generated. The inter-arrival time for distinct paths is exponentially distributed. The path amplitudes of CIR are Rician distributed in nature, with a 20 dB difference between the beginning and the end of the guard period. All paths in $[-b_{max}, b_{max}]$ have a uniform distribution of residual Doppler rates, thus channels with $b_{max} = 5 \times 10^{-4}$ and 1×10^{-3} are assumed to be various Doppler distorted. Because of the time-scale distortion, the normalized Doppler for UWA OFDM is based on the subcarrier frequency as each subcarrier has a different frequency shift. Further, According to Qarabaqi *et al*.,

Table 3 — OFDM parameters which used in simulations

Parameters	Values
Number of subcarriers	1024
Subcarrier spacing (Δf)	9.54kHz
Carrier frequency (f_c)	13.6kHz
Bandwidth (B)	9.77kHz
Number of nulls $\lvert S_N \rvert$	96
Number of pilot $\lvert S_P \rvert$	256
Guard time (T_g)	6.15ms
Pilot spacing	2, 4, 8

Table 4 — Underwater channel simulation parameters

Parameters	SPACE08
Surface height (depth) (h_0) [m]	100
Transmitter depth [m]	58
Receiver depth [m]	50
Bandwidth [kHz]	9
Carrier frequency [kHz]	13
Minimum frequency [kHz]	8.5
Roll-off factor	0.38
Time resolution [ms]	50
Frequency resolution [Hz]	25
Relative velocity (between Tx and Rx) [m/s]	0
Spreading factor	1.7
Distance between Tx and Rx [km]	1

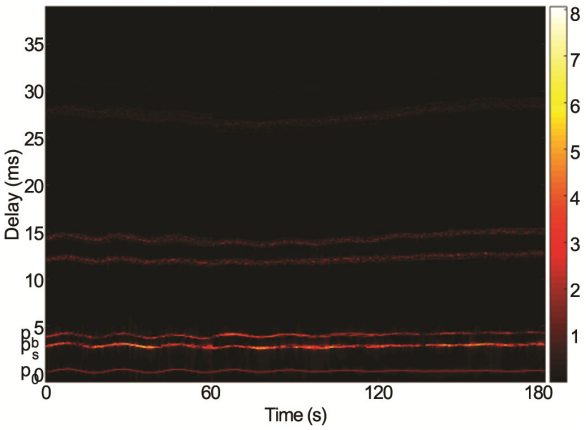

Fig. 3 — Acoustic Underwater CIR

the time-varying stochastic CIR has been simulated[30]. The CIR considers frequency-dependent attenuation, scattering of surface/bottom, and other random variations in the medium and source-receiver location. Using four distinct deployment locations with varying degrees of mobility, the authors found a strong match between their theoretical model and the data they acquired in the experiments.

It is difficult to construct an ideal pilot for high Doppler UWA channels. Channel coding is also used in real-world UWA communication systems to improve the receiver's error performance. To demonstrate the capability of the proposed channel estimation technique, we focused on the MSE and BER performance in an uncoded OFDM-based UWA communication system. A standard AOMP method first estimates the path delays and Doppler shifts. The AOMP-MAP technique is then used to estimate the complex-valued channel gains. According to the signal-to-noise ratio values, the number of Monte Carlo runs is raised as a function of SNR such that more Monte Carlo runs are performed as the SNR becomes larger. In order to do this, step size is set to 250, which is more than enough to get estimation errors of up to 10^{-5} with acceptable precision.

In Fig. 4 and 5, the BER and MSE performance of the OMP, AOMP, and AOMP-MAP algorithms in the presence of Doppler spread for 16QAM signaling formats as a function of SNR in the UWA channel have been shown. Also, the proposed technique is compared with previously reported FID[14] and LS[13] base techniques. During simulation, the Doppler spread and oversampling factor are set to 10×10^{-4} and 4 respectively. It can be observed from the plots that response of the FID[14] and LS[13] base techniques show a negligible change with respect to the SNR variation. On the other end, the MSE and BER performance of the OMP[24], AOMP, and AOMP-MAP algorithms show considerable drop as the SNR value is increased. Figures 4 and 5 show that the AOMP and AOMP-MAP approach consistently outperforms the OMP estimator due to its excellent channel estimation and BER performance. Another advantage of MVUE -based sparse channel recovery over OMP-based sparse channel recovery is that the BER curve is closer to the genie-aided data detection curve.

Compared to OMP[24], the AOMP-MSE based on MVUE method provides a better MSE in estimating the channel matrix. For pilot-only data, methods proposed by Huang *et al.*[13], Berger *et .al.*[14] , and

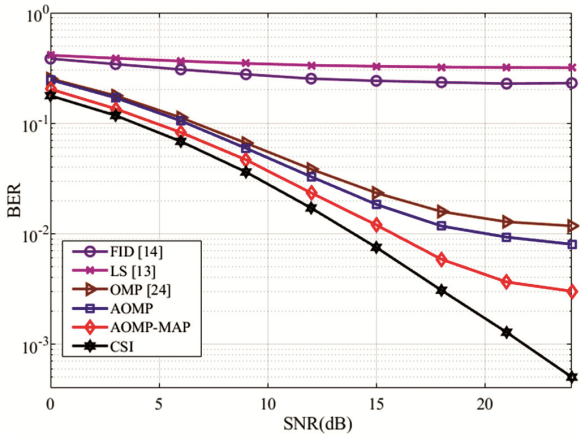

Fig. 4 — BER vs SNR where number of trials = 1000, b_{max} = 10^{-3}, mQAM = 4, number of partial interval=4, spacing of Doppler scale grids (β_p)= 0.667×10^{-4}.

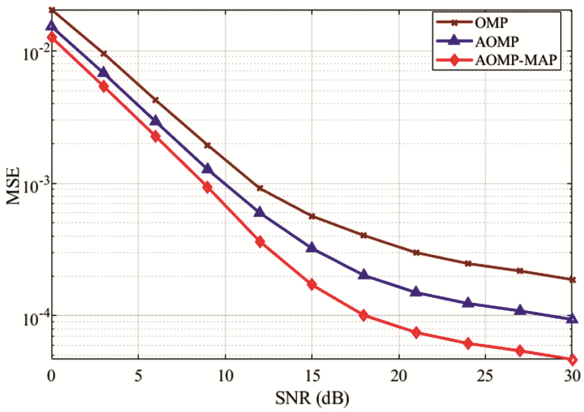

Fig. 5 — MSE vs SNR where b_{max} = 10^{-3}, mQAM = 4, number of partial interval=4, spacing of Doppler scale grids (β_p)= 0.667×10^{-4}.

Arunkumar *et al.*[24] that employ FID output exhibit their MSE performance in Fig. 5. Depending on the modulation scheme, the MSE performance of the AOMP-MAP algorithm is approximately -36dB better than the OMP method in the (25-30)dB SNR range. The same is compared with the AOMP algorithms, where the proposed AOMP-MAP algorithm is -40dB better in the range of (25-30)dB SNR. One of the reasons for this is because the AOMP-MAP algorithm makes efficient use of the prior knowledge from the Rician distributed channel gains. To identify data, the iterative approach described in this study outperforms previous techniques based on sparse channel recovery and least squares channel estimation at all SNRs.

As illustrated in Figs. 6 and 7, the AOMP-MAP, AOMP, and OMP algorithms are exhibited as functions of Doppler rate in terms of their MSE and

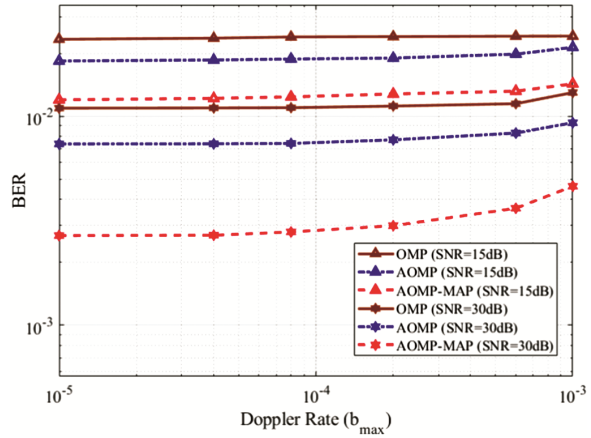

Fig. 6 — BER versues Doppler rate performance of OMP, AOMP, and AOMP-MAP algorithms when the Doppler scale is varied.

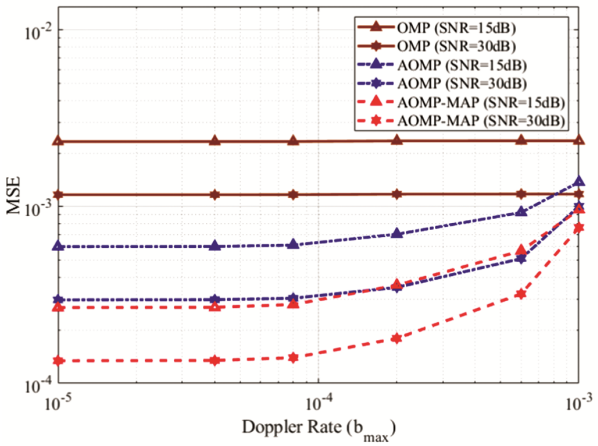

Fig. 7 — MSE versues Doppler rate performance of OMP, AOMP, and AOMP-MAP algorithms when the Doppler scale is varied.

BER performance. At zero Doppler spread, all methods perform almost identically. However, as the Doppler scale grows, the performance difference between the proposed scheme and other schemes increases, emphasizing the importance of PID-based channel estimation in high Doppler spread contexts. In Fig. 6, we can observe that the BER performance for adaptive based sparse reconstruction algorithms AOMP and AOMP-MAP is constant when $b_{max} = 6 \times 10^{-4}$ and 8×10^{-5} at SNR value equals to 15dB and 30dB respectively. After the BER performance decreases. Similarly, when $b_{max} = 8 \times 10^{-5}$ for all values of SNR, the performance of the MSE constant is advantageous for UWA communication.

Figures 8 and 9 show the BER and MSE performance comparison with the OMP, AOMP, AOMP-MAP algorithms. In Fig. 8, the performance

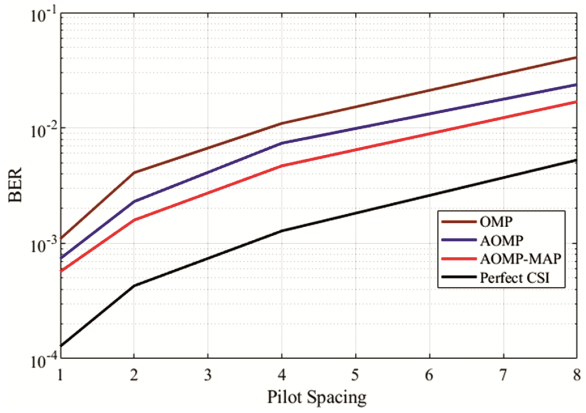

Fig. 8 — The BER performance comparision with the various sparse reconstruction algorithms, where SNR is set to 20dB.

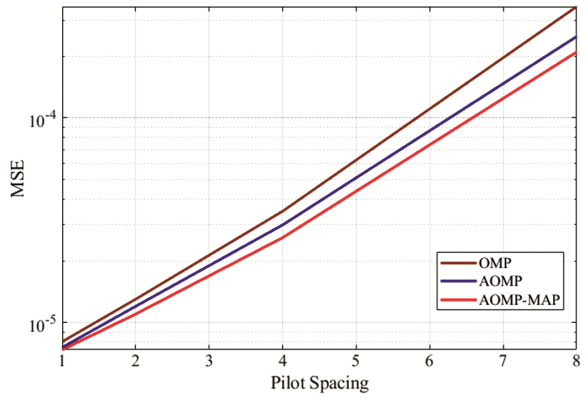

Fig. 9 — The MSE performance comparison with the various sparse reconstruction algorithms, where SNR is set to 20dB.

curves of BER are the same for all reconstructed sparse recovery algorithms. Better performance has been observed for the proposed AOMP-MAP algorithm. Similarly, the performance curve for MSE has been achieved. Numerically, the BER of the AOMP-MAP can be reduced up to 58.75% and 28.97% in the case of 8 pilots when using the same pilots of the OMP and AOMP, respectively. Nevertheless, the MSE in Fig. 9 can be reduced to 40.02% and 16.12% in the case of 8 pilots when using the exact parameters of sparse reconstructed algorithms OMP and AOMP, respectively. According to the observation, we can say that the AOMP-MAP is more sensitive to the pilot spacing.

Figures 10 and 11 shows the BER and MSE performance for the PFFT combiner using the banded MMSE equalizer from (36), as a function of SNR and the model parameters. In both the plots, it can be perceived that increment in the value of PID results in downshifting of the response curves, which indicates rapic decrease in the BER and MSE performance for rise

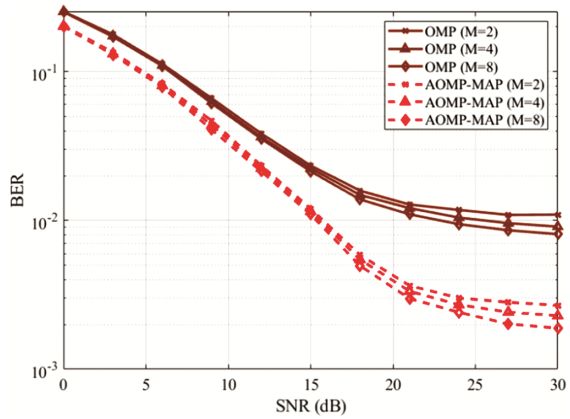

Fig. 10 — BER performance comparision of OMP, AOMP, AOMP-MAP algorithms and model parameters for the PFFT combiner, using the banded MMSE equalizer.

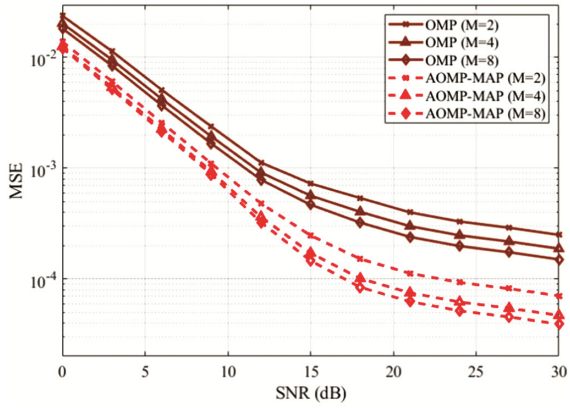

Fig. 11 — MSE performance comparison of OMP, AOMP, AOMP-MAP algorithms and model parameters for the PFFT combiner.

in the SNR values. Here Doppler spreading factor $b_{\max}$ is set to 10×10^{-4}. A time-varying channel has been assumed, which is well known for computing the PFFT combiner weights from (28). The Proposed AOMP-MAP algorithm's optimal sparse channel estimation performance may be observed in these graphs, which show that an oversampling factor of $M = 4$ is adequate. In addition, the BER curve of the MVUE -based sparse channel recovery is closer to that of the genie-aided data detection than the OMP-based sparse channel recovery technique. At an SNR of roughly 30 dB, the MVUE-based channel estimate achieves the CRB corresponding to PID observation better than any other sparse channel recovery schemes.

6 Conclusions

In this paper, sparse channel estimation and equalization for OFDM-based UWC have been presented. The time variations within the OFDM symbol length have been tracked using the PID measurements. The pilot-only measurement has been used for channel estimation and unknown data symbol detection. The termination conditions of the OMP algorithm has been the primary focus of our work in precise estimation of the UWA channel. Since, the noise has a significant impact on estimating accuracy as well as computing costs and that has led to recovery sparsity, so, in order to increase the estimation accuracy in high-level noise instances, we have generated a closed-form expression for the termination condition, referred to as the AOMP. The AOMP and MAP algorithms are combined to provide a computationally efficient and a new channel estimation scheme for determining the sparse complex channel path gain. The channel delays have been investigated by using the AOMP-MAP algorithm. The AOMP-MAP technique is used in this algorithm to estimate the unknown parameters of the UWA channel. Based on the minimum variance unbiased estimator (MVUE) algorithm, a sparse channel recovery scheme has also been introduced, which bootstraps and refines the AOMP's initial estimate. In order to evaluate the proposed algorithm's performance, comprehensive computer simulations using simulated data relating to existing SPACE08 underwater channel environmental condition are executed. Simulation results reveal that the BER of the AOMP-MAP gets reduced to 58.75%, and 28.97% and the MSE of the AOMP-MAP reduces to 40.02% , 16.12% in the case of 8 pilot system, when same pilots of the OMP and AOMP have been used. Based on the suggested approach, UWA channel estimation performance is found outstanding in these computer simulations and resulted in extremely low BER and MSE. In this way, the proposed technique and subsequent channel estimation algorithm are quite promising for this type of complex and demanding channel estimation scenario.

Acknowledgments

The authors are grateful for the funding support of the Science and Engineering Research Board (SERB), Department of Science & Technology (DST), Government of India, vide file no. is SRG/2020/002486.

References

1 Chen Y, Clemente C & Soraghan J, *J Infect,* 12 (2021) 469.
2 Javaid N, Ahmad Z, Sher A, Wadud Z, Khan Z A & Ahmed S H, *J Ambient Intell Humaniz. Comput,*10 (2019) 4225.

3 Chen P, Rong Y, Nordholm S & He Z *IEEE Trans Veh Technol,* 66 (2017) 10567.
4 Taubock G, Hlawatsch F, Eiwen D & Rauhut H, *IEEE J Sel Top Signal Process,* 4 (2010) 255.
5 Abdzadeh-Ziabari H, Zhu W P & Swamy M N S, *IEEE Trans Veh Technol,* 67 (2018) 2787.
6 Zhou Y H, Tong F & Zhang G Q, *Appl Acoust,* 117 (2017) 160.
7 Yan Z, Yang X, Sun L & Wang, *J China Commun,* 18 (2021) 216.
8 Wan L, Jia H, Zhou F, Muzzammil M, Li T & Huang Y, *Signal Processing,*170 (2020) 107439.
9 Wan L, Qiang X, Ma L, Song Q & Qiao G, *IEEE Wirel Commun Lett,* 8 (2019) 117.
10 Peng B, Rossi P S, Dong H & Kansanen K, *IEEE Commun Lett,* 19 (2015) 1081.
11 Ahmed S, *Ocean 2015 - MTS/IEEE Washingt,* (2016).
12 Sifferlen J F, Song H C, Hodgkiss W S, Kuperman W A & Stevenson J M, *IEEE J Ocean Eng,* 33 (2008) 182.
13 Huang J, Zhou S, Huang J, Berger C R & Willett P, *IEEE J Sel Top Signal Process,* 5 (2011) 1524.
14 Berger C R, Zhou S, Preisig J C & Willett P, *IEEE Trans. Signal Process,* 58 (2010) 1708.
15 Yerramalli S, Stojanovic M & Mitra U, *IEEE Trans Signal Process,* 60 (2012) 5906.
16 Li Y, Sha X & Wang K, *IEEE Commun Lett,*17 (2013) 2260.
17 Tu K, Fertonani D, Duman T M, Stojanovic M, Proakis J G & Hursky P, *IEEE J Ocean Eng,* 36 (2011) 156.
18 Han J, Zhang L & Leus G, *IEEE Signal Process Lett,* 23 (2016) 282.
19 Yang Z & Zheng Y R, *IEEE J Ocean Eng,* 41 (2016) 232.
20 Chen Z, Wang J & Zheng Y R, *IEEE J Ocean Eng,* 42 (2017) 711.
21 Qin X, Qu F & Zheng Y R, *IEEE J Ocean Eng,* 46 (2021) 326.
22 Tao J, Zheng Y R, Xiao C & Yang T C, *IEEE J Ocean Eng,* 35 (2010) 948.
23 Rafati A, Lou H & Xiao C, *IEEE J Ocean Eng,* 39 (2014) 90.
24 Arunkumar K P & Murthy C R, *IEEE Trans Signal Process,* 66 (2018) 5041.
25 Mason S F, Berger C R, Member S, Zhou S & Willett P, *IEEE J Sel Areas Commun*, 26 (2008) 1638.
26 Kumar A & Kumar P, *5th Int Conf Comput, Commun Security*, (ICCCS) (2020).
27 Panayirci E, Senol H, Uysal M & Poor H V, *IEEE Trans Signal Process,*64 (2016) 214.
28 Yin J, Ge W, Han X, Liu B & Guo L, *IEEE Commun Lett,* 23 (2019) 2086.
29 Panayirci E, Altabbaa M T, Uysal M & Poor H V, *IEEE Trans Signal Process,*67 (2019) 1550.
30 Qarabaqi P & Stojanovic M, *IEEE J Ocean Eng,* 38 (2013) 701.
31 Liu C, Zakharov Y V & Chen T, *IEEE Trans Veh Technol,* 61 (2012) 938.
32 Walree P A V, Socheleau F X, Otnes R & Jenserud T, *IEEE J Ocean Eng,* 42 (2017) 1007.
33 Fang K, Rugini L & Leus G, *IEEE Trans Signal Process,* 56 (2008) 5555.
34 Wang Z, Li Y, Wang C, Ouyang D & Huang Y, *IEEE Wirel Commun Lett,* 10 (2021) 1761.
35 Kay S M & Englewood C N J, Prentice-Hall, (1988).
36 Berger C R, Wang Z, Huang J & Zhou S, *IEEE Commun Mag,* 48 (2010) 164.
37 Li C, Song K & Yang L, *IET Commun,*11 (2017) 1143.
38 Huang Y, Wan L, Zhou S, Wang Z & Huang J, *Phys Commun,*13 (2014) 156.
39 Kumar A & Kumar P, *ETRI Journal*,(2022) 1.